L-Band Radar Soil Moisture Retrieval Without Ancillary Information

Cintia A. Bruscantini, *Student Member, IEEE*, Alexandra G. Konings, *Student Member, IEEE*, Parag S. Narvekar, *Member, IEEE*, Kaighin A. McColl, *Student Member, IEEE*, Dara Entekhabi, *Senior Member, IEEE*, Francisco M. Grings, *Member, IEEE*, and Haydee Karszenbaum, *Member, IEEE*

***Abstract*—A radar-only retrieval algorithm for soil moisture mapping is applied to L-band scatterometer measurements from the Aquarius. The algorithm is based on a nonlinear relation between L-band backscatter and volumetric soil moisture and does not require ancillary information on the surface, e.g., land classification, vegetation canopy, surface roughness, etc. It is based on the definition of three limiting cases or end-members: 1) smooth bare soil; 2) rough bare soil; and 3) maximum vegetation condition. In this study, an estimation method is proposed for the end-member parameters that is iterative and only uses space-borne measurements. The major advantages of the algorithm include an analytic formulation (direct inversion possible), and the fact that there is no requirement for ancillary information. Ancillary data often misclassify the surface and the parameterizations linking surface classification to model parameter values are often highly uncertain. The retrieval algorithm is tested using 3 years of space-borne scatterometer observations from the Aquarius/SAC-D. Retrieved soil moisture accuracy is assessed in several ways: comparison of global spatial patterns with other available soil moisture products (two reanalysis modeling products and retrievals based on the Aquarius radiometer), extended triple collocation (ETC) and time series analysis over selected target areas. In general, low bias and standard deviation are observed with levels comparable to independent radiometer-based retrievals. The errors, however, increase across areas with high vegetation density. The results are promising and applicable to forthcoming L-band radar missions such as SMAP-NASA (2015) and SAOCOM-CONAE (2016).**

***Index Terms*—Aquarius/SAC-D, microwave remote sensing, radar, radar roughness, radar vegetation index (RVI), scatterometer, soil moisture.**

I. Introduction

SOIL moisture is an essential climate variable for meteorological, ecological, agricultural, and hydrological applications. As a state variable of the terrestrial branch of the water cycle, soil moisture information is a relevant input in all the process models regarding these disciplines. Microwave remote sensing observations can provide valuable mapping information of soil moisture (m_v). Microwave emission at L-band is sensitive to soil moisture and is not much influenced by vegetation. However, their low spatial resolution (of the order of tens of kilometers) makes them not suitable for agricultural applications. Although radar achieve higher resolutions, the radar signal is more influenced by surface roughness, vegetation, and topographic effects.

Past studies provide evidence that L-band backscatter, especially in copolarized channels, is sensitive to soil moisture. However, it is also influenced by vegetation through volume scattering and multiple scattering. It is also sensitive to surface roughness. A major challenge for retrieving soil moisture from backscatter observations is isolating these roughness and vegetation contributions. Land parameter retrieval from remote sensing observations is a typical ill-posed problem mainly because the number of unknown parameters is higher than the number of independent satellite observations, and because there is no obvious relation between electromagnetic response and land parameters. Narvekar *et al.* [1] and Kornelsen and Coulibaly [2] provide a summary of existing approaches to surface soil moisture retrieval using active microwave observations. The review identifies the major types of approaches and lists the ancillary data needed to reduce the number of unknowns in the retrieval. Ancillary information is all the information derived from other than the observing system (in this work, the Aquarius scatterometer). One approach that stands out for surface soil moisture retrieval without extensive ancillary data needs is the time-series approach. One possible solution for resolving the ambiguity is proposed in Kim *et al.* [3]. It is based on the assumption that there is a separation of time scales in soil roughness and soil moisture variations. This leads to the constraint that soil roughness is constant in a relatively short time window and reduces the number of unknowns in the retrieval when multitemporal observations are available.

Other approaches that rely on inverse scattering models require ancillary information that may not be reliable or available at global scale. Some m_v retrieval algorithms rely on complex forward models, such as numerical Maxwell model in three dimensions (NMM3-D) [4] and Tor Vergata active/passive model [5], that are based on rigorous scattering theory that links surface parameters and radar observations, and takes into consideration several dielectric and geometric properties of the scenes to evaluate the backscatter. However, these forward models cannot be analytically inverted or used for global

Manuscript received December 5, 2014; revised October 20, 2015; accepted October 23, 2015. Date of publication November 19, 2015; date of current version January 25, 2016.

C. A. Bruscantini, F. M. Grings, and H. Karszenbaum are with the Department of Remote Sensing, Institute of Astronomy and Space Physics (IAFE), Ciudad de Buenos Aires 1428, Argentina (e-mail: cintiab@iafe.uba.ar).

A. G. Konings, P. S. Narvekar, K. A. McColl, and D. Entekhabi are with the Department of Civil and Environmental Engineering, Massachusetts Institute of Technology, Cambridge, MA 02143 USA (e-mail: konings@mit.edu).

Color versions of one or more of the figures in this paper are available online at http://ieeexplore.ieee.org.

Digital Object Identifier 10.1109/JSTARS.2015.2496326

real-time retrievals because they are computationally intensive. Moreover, the required ancillary information cannot be provided at a global scale. Thus, the forward model is computed for canonical land covers to generate loop-up tables. The choice of dominant land classification (and hence data cube choice) is based on an ancillary land use classification. These simplifications are all error sources that will decrease the retrieval reliability.

Other retrieval algorithms include semiempirical or empirical approaches. Whereas empirical models [6], [7] estimate the backscatter and soil parameters relation statistically from databases acquired during field campaigns, semiempirical models are partially physically based and then use simulated or experimental datasets to simplify the model. Examples of semiempirical models include Oh *et al.* [8], Dubois *et al.* [9], and Shi *et al.* [10]. However, these models have the drawback of having limited applicability outside the range of data and conditions for which they were derived.

Finally, retrieval algorithms based on artificial neural networks can be trained exploiting the synergy between electromagnetic scattering models and experimental data obtained during field campaigns, such as the one described in [11].

A radar-only soil moisture retrieval algorithm is derived by Narvekar *et al.* [1]. It has been evaluated using radar observations gathered in several field campaigns [1]. The algorithm is based on the definition of three end-members: 1) smooth bare soil; 2) rough bare soil; and 3) maximum vegetation condition. There are global parameters associated with these end-members. The degree of roughness and vegetation volume relative to these end-members at each location and time determines the retrieval parameters for the data granule. These spatially and temporally variable roughness and vegetation levels are estimated from combinations of copolarized backscattering channels to avoid the need for ancillary information. Information derived from other sensors and ground sampling is considered to be a major source of error in retrieval algorithms. For example, land use classification derived from optical data is not only noncontemporaneous, but requires strong assumptions linking optical properties of a plant canopy to its microwave electromagnetic effects. Other ancillary data sources like soil texture classification are based on limited and sporadic ground sample and they are categorical. In this study, we aim to develop a radar-based surface soil moisture mapping capability that does not need such problematic ancillary data and that can use the radar measurements themselves to distinguish between vegetation, surface roughness, and soil dielectric constant contributions to the polarimetric backscatter measurements.

The radar-only algorithm is mathematically simple and it can be inverted analytically, making it applicable for quick-look and near real-time global-scale retrievals. The main drawback of the algorithm is that it depends on global parameters that capture limiting conditions (i.e., end-members). Narvekar *et al.* tested the algorithm on field campaigns and used available ground measurements in order to calibrate the parameter values. However, these end-member values may not apply at larger scales, as will be shown later on in Section II-C. Therefore, in this study, a modification of the end-member parameter estimation approach is introduced in order to allow the algorithm to be applicable at satellite sensing scales and without the use of ancillary data. Instead of calibrating the end-members values through ground measurements (which is not feasible at satellite sensing scales), we introduce an iterative procedure that only uses the radar observations. The proposed algorithm is applied to L-band backscatter observations from the Aquarius/SAC-D covering the globe over 3 years. The main drawback of the Aquarius scatterometer is its coarse spatial resolution (about 100 km). The Aquarius data were used in this analysis because it is the only spaceborne L-band radar data currently available at three polarizations (HH, VV, and HV). This study is a proof-of-concept for the higher resolution SMAP and the SAOCOM L-band missions. The main scientific objective of these forthcoming missions is soil moisture monitoring at significantly higher resolution: SMAP from 1 to 3 km and SAOCOM better than 1 km. Derivation of surface soil moisture information from high resolution radars still faces the challenge to isolate roughness, vegetation, and soil moisture from backscatter observations. The use of polarization information to isolate these effects is directed toward the application of these forthcoming missions to the surface soil moisture mapping problem. A major shortcoming of using the coarse-resolution Aquarius data in the proof-of-concept is that low resolution radars is associated with a mix of scattering mechanisms within the footprint.

The m_v retrievals are evaluated using reanalysis (models forced with micrometeorological forcing) products and a soil moisture product based on retrieval with the Aquarius radiometer, an independent estimate. Triple collocation (TC) is used to estimate the standard deviation of errors in each of the three surface soil moisture data sources. The retrieval algorithm also allows the estimation of the time-varying partial contributions of effective surface roughness, vegetation volume scattering, and surface reflection to the total backscatter. The partitioning information is relevant to relative index soil moisture algorithms that use backscatter variations between a minimum and maximum value to isolate surface soil moisture information in backscatter.

The study is structured as follows. First, the radar-only algorithm is briefly described in Section II-A. An overview of the Aquarius dataset used is presented in Section II-B. Our proposed modification for its initial parameter estimation is further discussed in Section II-C. In Section III, the algorithm is evaluated and contrasted to available m_v products considering both spatial patterns (global temporal averaged maps) and temporal behavior (extended triple collocation (ETC) of m_v anomalies and m_v time series at selected focus regions). Finally, results are discussed in Section IV.

II. Data and Methods

A. Retrieval Algorithm

A retrieval algorithm for surface soil moisture estimation using L-band radar observations is developed in [1]. It captures the nonlinear dependency between backscatter and m_v in a parameterized approach using the dependency

$$\sigma_{VV}(\text{ dB}) = \text{Sensitivity} * m_v^{\lambda} + \text{Intercept} \tag{1}$$

where λ is the parameter capturing the nonlinearity. The *Sensitivity* and *Intercept* parameters depend on surface roughness and vegetation volume. The three parameters (λ, *Sensitivity*, and *Intercept*) vary for each location and each overpass depending on the local conditions related to vegetation and soil characteristics. In the algorithm these parameters are determined by scaling among three end-members: 1) smooth bare soil; 2) rough bare soil; and 3) maximum vegetation condition. There are global parameters associated with these end-members. For each location and time, the locally applicable parameters are determined by scaling between the end-members using two radar-derived indices. The first is for vegetation. The radar vegetation index (RVI) [12] is defined as

$$RVI = \frac{8\sigma_{HV}}{\sigma_{HH} + \sigma_{VV} + 2\sigma_{HV}} \quad (2)$$

where σ are in linear units. RVI generally varies from 0 for bare soil to 1, or higher, for fully vegetated areas. The RVI index is a measure of randomness of the scatterers, hence is related to structural components of vegetation canopies (volume scattering), which are indirectly related to vegetation water content. The RVI index is indicative of vegetation volume scattering only if there are no surface contributions and vegetation canopy is composed of random infinitely long lossy dielectric cylinders [13]. Although RVI is independent of vegetation greenness, Yueh *et al.* [14] reported a high correlation (0.9) between RVI and vegetation opacity derived using PALS radar observations. There are some limitations of using RVI as a proxy of vegetation cover. First, RVI is also a function of incidence angle, since the path length through the canopy changes with observation geometry [3]. Moreover, McColl *et al.* [15] reported an overestimation of Aquarius-RVI-derived biomass over dry regions possibly due to calibration errors on σ_{HV}. Advantages of using RVI as a metric of vegetation cover include the following: 1) simple index; 2) does not rely on ancillary data derived from other observing systems; 3) temporally and spatially collocated with the soil moisture estimate; and 4) low sensitivity to environmental condition effects.

To avoid reliance on ancillary information of soil roughness, Narvekar *et al.* introduced a new radar roughness index (RRI) to estimate ks (with $k = 2\pi/L$, L radar wavelength, and s soil rms height) defined as

$$RRI = \frac{\sigma_{HH} - \sigma^{s}_{HH}}{\sigma_{VV} - \sigma^{s}_{VV}} \quad (3)$$

where σ^{s}_{HH} and σ^{s}_{VV} are *Intercept* for smooth bare soil.

Exploiting numerical scattering models results [16], the following polynomial function was fitted between RRI and ks:

$$RRI = 0.3034ks^3 - 0.9203ks^2 + 0.9989ks + 0.3910. \quad (4)$$

The polynomial fit between RRI and ks was developed using available data library on the numerical solutions of the Maxwell equation (see [1]). Soil surface roughness effects are only partially captured with ks. The spatial correlations, e.g., also have a strong effect. The parameter ks thus cannot capture the full impacts of roughness on backscatter. The copolarization ratio is not uniquely related to ks as well. RRI is a limited diagnostic of the roughness contribution.

The retrieval algorithm depicted in (1) uses VV polarization. *Sensitivity* and *Intercept* are based on the definition of three limiting cases or end-members.

Sensitivity is the ratio between $\sigma\,(\mathrm{dB})$ and m_v variations, and it varies with vegetation density and soil roughness. Observations of σ_{VV} over bare soil are expected to have the highest sensitivity to m_v; *Sensitivity* decreases with higher vegetation density because of signal attenuation due to the vegetation layer [17]. Thus, it is expected that *Sensitivity* values will drop with RVI. Similarly, *Sensitivity* increases with increasing soil roughness [18]. Some rough surface scattering models such as the small perturbation method and the Oh model [19] predict a decoupling between roughness and dielectric constant terms, thus resulting in radar sensitivity to m_v independent on soil roughness. However, observations presented in Wang *et al.* [20] and Ulaby and Batlivala [21] show that roughness increases *Sensitivity*. In the latter work, it was observed that roughness changes *Sensitivity* in moderate vegetation. A conceptual figure of *Sensitivity* versus RVI and rough-to-smooth soil transition may be drawn and it takes a shape defined by three vertices (end-points) such as the one shown in the inset of Fig. 1(a). The shape end-points are the *Sensitivity* values of the three end-members. Bare soil end-members are at the lowest vegetation level (RVI tends to zero). Smooth bare surfaces (first end-member) correspond to the lowest *Sensitivity* end-point on the bare soil edge of the shape. As the roughness of the surface increases, so does the *Sensitivity*. Hence, the second end-member is located in the opposite end of the bare soil edge. Finally, over maximum vegetation regions (third end-member), *Sensitivity* drops to its minimum value, thus closing the shape at the high RVI end point.

Intercept is the backscatter expected over dry soils. Similar to *Sensitivity*, *Intercept* $\sigma\,(\mathrm{dB})$ relates to vegetation density and soil roughness. However, unlike *Sensitivity*, *Intercept* increases with vegetation due to backscatter contribution of the vegetation cover [17]. In the same way, soil roughness contributes to increase σ_{VV}, and hence *Intercept* value. Therefore, *Intercept* versus RVI should also resemble a shape defined by three vertices similar to the *Sensitivity* shape but flipped upside down [see inset in Fig. 1(b)].

Narvekar *et al.* [1] use RVI to scale the *Sensitivity* and *Intercept* parameters between the end-members for every observation in space and time. Furthermore, they apply the estimated roughness ks based on RRI (4) to correct for surface roughness contributions. The resulting single-equation algorithm is

$$\begin{aligned}\sigma_{VV} = \{&RVI\gamma + (1 - RVI)[1 + \log(1 + ks)]S_s\}m_v^{\lambda} \\ &+ RVI\sigma^{vf}_{VV} + (1 - RVI)[\sigma^{s}_{VV} + C\log(1 + ks)] \quad (5)\end{aligned}$$

where S_s and γ are the *Sensitivities* for smooth bare soil and maximum vegetation end-members, σ^{vf}_{VV} and σ^{s}_{VV} are their corresponding *Intercepts* and C is a constant value (fixed to 13.6). Narvekar *et al.* [1] provide details of the algorithm development. It is noteworthy that this retrieval algorithm (5) is invertible and does not require any ancillary information.

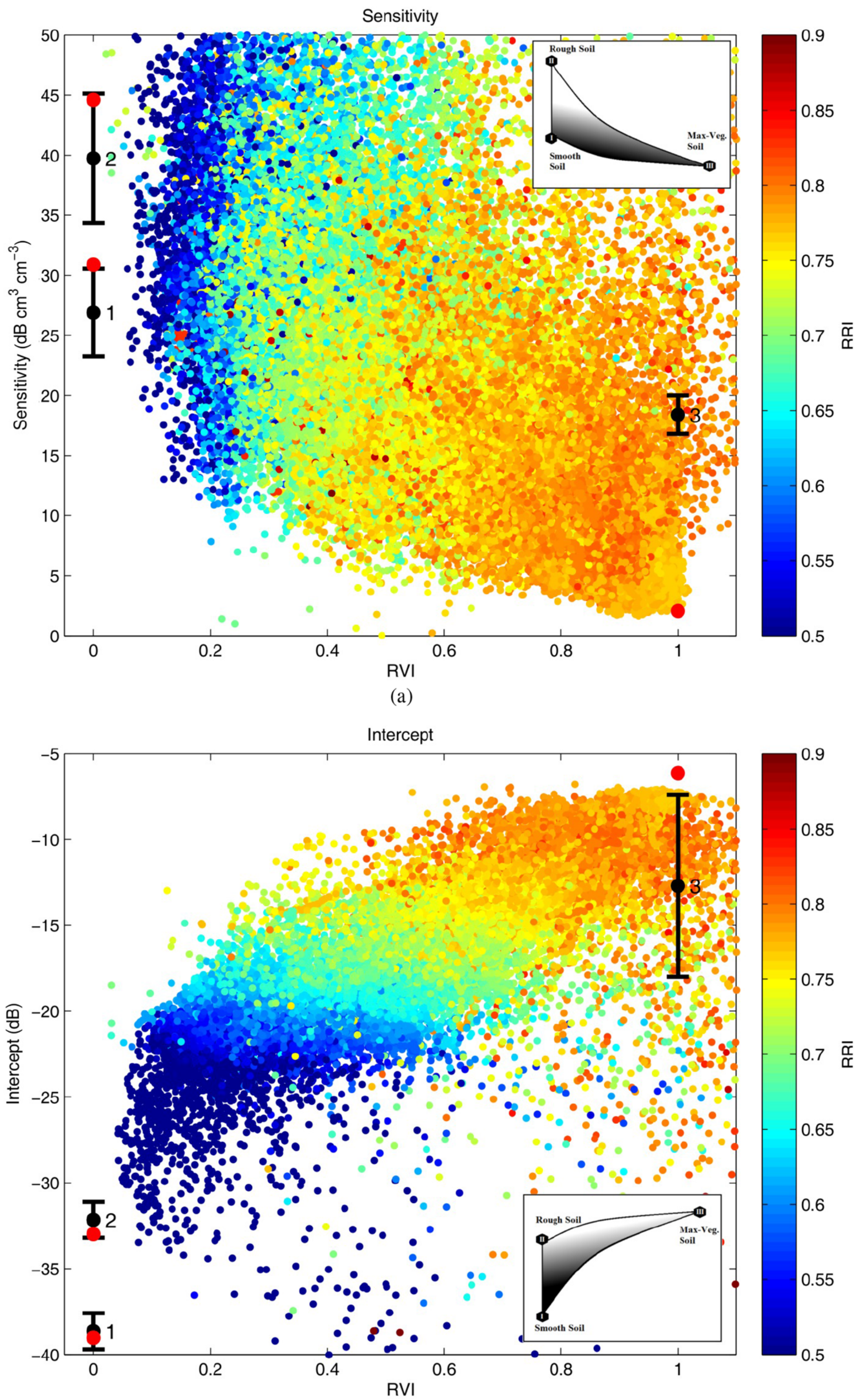

Fig. 1. (a) *Sensitivity* and (b) *Intercept* parameters versus RVI. *Sensitivity* (*Intercept*) decreases (increases) with increasing vegetation level. Color levels represent RRI values. Black bars indicate *Sensitivity* range obtained from field experiments for three end-members. 1) Smooth bare soil. 2) Rough bare soil. 3) Maximum vegetated areas. Red dots indicate the end-points estimated using the Aquarius data. Inset figures are conceptual shapes defined by three vertices, expected from theory.

Consequently, using (2) and (5), together with end-member parametrization, it is possible to estimate m_v and ks using solely σ_{HH}, σ_{HV}, and σ_{VV}.

In order to test if the conceptual shapes are found in observations, the Aquarius scatterometer measurements are used. These measurements are used for illustrative purposes only here and will be discussed in Section II-B. *Sensitivity* is computed at each pixel as an approximation of $\Delta\sigma_{VV}(\mathrm{dB})/\Delta \mathrm{m_v}$. At each pixel, Δm_v is obtained using m_v retrieved applying the methodology explained in Section II-C.

Sensitivity varies with vegetation and soil roughness, thus it changes over time at each pixel. The *Sensitivity*

$\Delta\sigma_{VV}(\mathrm{dB})/\Delta \mathrm{m_v}$ is computed for each pixel and plotted against the temporally averaged RVI for 3 years of the Aquarius data and for all global land pixels (excluding frozen surfaces). These data shown in Fig. 1(a) are also color-coded with the corresponding RRI or index of roughness. End-members obtained by Narvekar *et al.* using field experiment measurements are indicated in the figure as black bars that span the range of *Sensitivity* optimized for each of the five campaigns. Moreover, red large dots indicate the end-points estimated using the Aquarius data and our proposed iterative algorithm (see Section II-C for further details). The Aquarius data are concentrated in a shape that resembles the conceptual inset figure. *Sensitivity* approaches zero for dense canopy cover (high RVI), as expected. For surfaces with low vegetation cover, the more rough surfaces have greater *Sensitivity* magnitudes. It is also evident that vegetation also induces increases in the roughness parameter. Therefore, the roughness index must be interpreted as an effective roughness that is due to both soil surface and vegetation canopy volume (more discussion below in Section III-A).

Intercept is computed at each pixel as the temporal minimum of the Aquarius measurements of $\sigma_{VV}(\mathrm{dB})$. *Intercept* is plotted against mean RVI at each pixel and results are shown in Fig. 1(b). Recall that the *Intercept* is the $\sigma_{VV}(\mathrm{dB})$ expected over dry soils, thus finding the minimum $\sigma_{VV}(\mathrm{dB})$ at each pixel may not be a good approximation of *Intercept* values for pixels that are not dry. Moist pixels contribute to overestimate *Intercept* values. Thus, pixels with minimum temporal m_v values higher than 0.05 $\mathrm{cm^3/cm^3}$ should be filtered out if there is some previous knowledge of m_v values. As will be shown in the iterative algorithm described in Section II-C, at every iteration, a new m_v retrieval is performed and it is used in the subsequent iteration for filtering pixels considered to be in dry state.

B. Aquarius/SAC-D

The Aquarius scatterometer provides backscattering observations at HH, HV, VV, and VH polarization with three different beams arranged in a pushbroom configuration at different incidence angles (28.8°, 37.9°, and 45.5°). The radar-only soil moisture retrieval algorithm is of particular interest for the SMAP mission; therefore, the Aquarius middle beam (37.9°) was selected in this study given its proximity to SMAP's incidence angle (40°). For this analysis, the Aquarius L2 version 2.0 of radar backscatter σ_{HH}, σ_{HV}, and σ_{VV} was used from August 25, 2011 to May 1, 2014. Observations were screened out using quality flags provided with the data. Given the Aquarius's 7-day revisit period, all data were gridded at the footprint scale using the first 7 days of footprints to define the grid. Gridding was carried out by nearest neighbor interpolation and observations with distance higher than 0.05° from the grid-cell centroid were excluded. Further details on the grid are described in [15].

C. Iterative End-Members Estimation

Using L-band backscatter observations and m_v acquired during several field campaigns (SGP99, SMEX02, CLASIC07, SMAPVEX08, and SMAPVEX12), Narvekar *et al.* [1] calibrated the proposed retrieval algorithm by finding, for each field campaign, the optimum end-member *Sensitivity* and *Intercept* parameters that minimized the retrieved m_v root-mean-square error (RMSE). However, applying nominal end-members proposed by Narvekar *et al.* [1] to the Aquarius dataset would not necessarily yield consistent retrievals. The spatial resolution and diversity of surface types are not the same between global observations of the Aquarius and the five field campaigns.

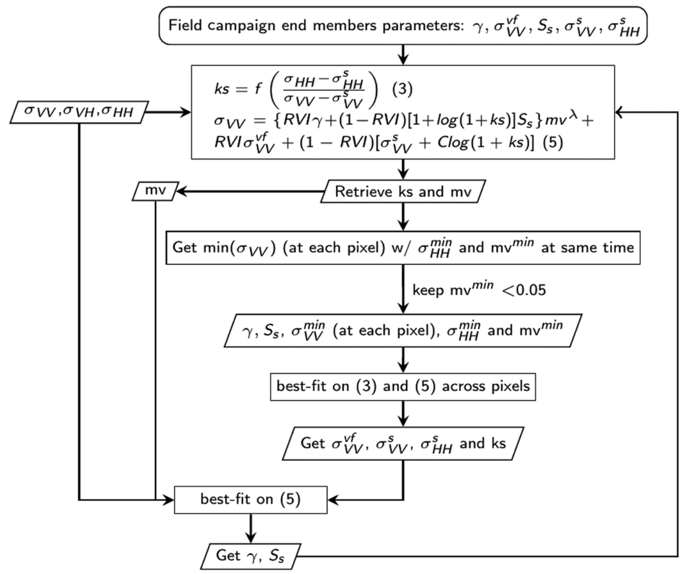

Fig. 2. Conceptual flow diagram of the iterative process parameter estimation (*Intercept* and *Sensitivity*). Note that no use of ancillary data is required.

Global calibration of the algorithm as done in Narvekar *et al.* at the Aquarius footprint resolution is not feasible because ground soil moisture data are not available at such coarse scale. In this study, the estimation of the Aquarius end-member parameters is performed through an iterative procedure. The procedure again does not require ancillary information and uses only the radar measurements. This method is applicable to other radar mission data such as the SMAP and the SAOCOM missions. The general idea behind the optimization of the parameter values is to find the three end-points that will place most of the data points inside the shape traced with the prior iteration end-points (see Fig. 1). However, note that the *Sensitivity* shape depends on the intra-pixel range of retrieved m_v and, consequently, on the three end-points found in the previous iteration.

The iteration flowchart is shown in Fig. 2. The iteration process consists of the following steps: A preliminary retrieval of m_v and ks is performed using an initial guess of the end-members parameters and (2)–(5). Using just the pixels that are considered dry, i.e., m_v below 0.05 $\mathrm{cm^3/cm^3}$, the temporal minimum σ_{VV} is obtained at each pixel (σ_{VV}^{min}). The *Intercept* parameters and ks are estimated by minimizing the difference between σ_{VV}^{min} at each pixel and modeled σ_{VV} considering (3)–(5), limiting the range of ks between 0.14 and 1.5, and using the initial guess of the *Sensitivity* parameters, σ_{VV}^{min}, m_v retrieved and σ_{HH} measured when σ_{VV}=σ_{VV}^{min}. At the final stage, S_s and γ are estimated using (5), *Intercept* values estimated in

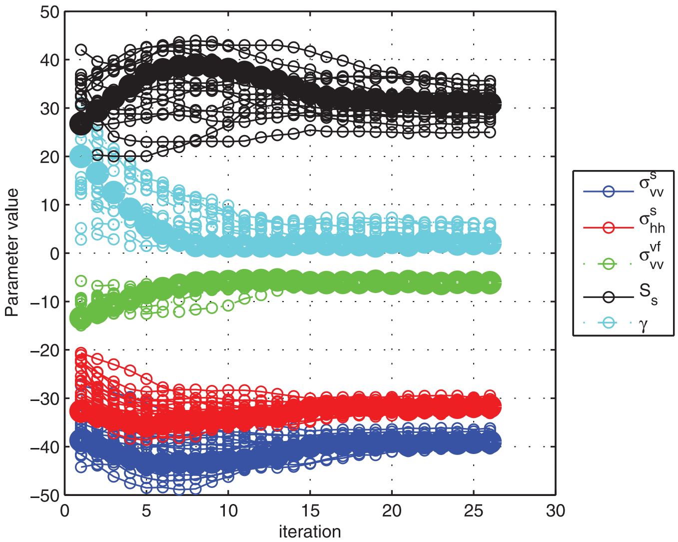

Fig. 3. Parameter values (dB) versus iteration using random initialization of the end-member parameters showing rate of convergence and stability when converged. It also shows compensation between correlated parameters.

the previous step, and retrieved values of ks and m_v. Given these new *Sensitivity* and *Intercept* values, the iterative process continues until parameters progressively converge.

The iterative nature of the methodology developed is related to the fact that the nonlinear cost function that is minimized depends on several free parameters, some of them are globally constant (end-members parameters) and others change from pixel to pixel and with time (m_v and ks). However, the set of measurements is monodimensional (σ_{VV}). In order to examine the robustness of the procedure, a set of random initial guess values was tested for convergence. The range considered for each end-member initial guess intends to extend the range of expected end-member values from theory and field campaigns [1]. Fig. 3 shows the iteration results for each initial guess. Overall, the iteration converges to a stable set of global parameters. The final set of parameters of the thicker line plot are used to retrieve m_v and ks using the 3 years of global measurements of the Aquarius. The robustness of the converged end-member parameters to the initial guess values is further analyzed in Section III-D.

This methodology is intended to estimate end-member parameter values from the statistics of the backscatter data, with the goal of retrieving m_v and ks using σ_{HH}, σ_{HV}, and σ_{VV}. The proposed iterative approach starts from a random initial guess of the end-members and converges to the optimum end-member values given the statistics of the dataset [red dots in Fig. 1(a) and 1(b)]. It is evident from the results that the iteration procedure tunes the end-member values to better accommodate the data points inside the delineated three vertices shapes. Note that the algorithm does not require ancillary data and is readily applicable to other missions and airborne data.

III. Results

Evaluation and validation of the retrieval algorithm presented in this study require ground-based measurements at the Aquarius footprint scale. However, there are no ground-based networks available that will cover such a coarse scale. As a result, we follow alternative evaluation methods that are appropriate and applicable in the given conditions. Evaluation of the performance of the radar-only algorithm is carried out by comparing retrieved m_v (m_v radar) with two soil moisture products: 1) the Aquarius L2 swath single orbit retrieval soil moisture version 2 retrieved using the single channel algorithm and horizontal brightness temperature observations (m_v radiometer) [22]; and 2) NASA global modeling and assimilation office (GMAO) reanalysis soil moisture (referred to hereafter as m_v GMAO). The latter is the m_v product derived from the SMAP Nature Run version 3 [23], which is a variant of the MERRA-Land (Modern-Era Retrospective Analysis for Research and Applications) reanalysis for the satellite era [24]–[26].

The Aquarius scatterometer and radiometer observations are simultaneously collocated, thus footprint to footprint comparison is straightforward. However, GMAO m_v had to be gridded to the Aquarius coarse resolution grid in order to carry out the comparison.

We perform three-way comparisons between the products using standard and basic approaches like scatterplots (in the form of boxplots for ease of visualization). But because the three data sources on the same variable (soil moisture) are derived from nonshared sources, namely the radar instrument, the radiometer instrument, and MERRA atmospheric forcing, their individual random errors are independent. As a result, TC can be used to estimate the standard deviation [27] and correlation coefficient [28] of the radar- and radiometer-based retrievals with respect to the unknown truth.

Fig. 4 shows direct comparison of the three m_v products in the form of boxplots. Boxplot intervals were selected so that the majority of the boxes would have the same number of paired m_v observations (approximately 200 000 data points each). Radar m_v shows a nonlinear bias toward lower m_v values as GMAO m_v increases beyond 0.25 $\mathrm{cm}^3/\mathrm{cm}^3$, whereas dry GMAO pixels display slightly lower values than radar. Radiometer m_v exhibits an overall negative bias when compared to GMAO m_v. Finally, when both Aquarius m_v products are compared, radiometer m_v values are lower than radar ones for $m_v < 0.2\ \mathrm{cm}^3/\mathrm{cm}^3$, and the opposite was found for pixels with $m_v > 0.2\ \mathrm{cm}^3/\mathrm{cm}^3$. The boxplots also show the 25 th and 75 th percentiles as well as minimum and maximum values in each bin. Although the medians in different bins between all three data source pairs compare well and follow monotonically (positive) relations when compared to each other, the percentiles and extrema show that there are considerable errors (both noise and bias) that may depend on surface characteristics. In order to examine the dependence on surface characteristics, temporal averages of the data products are mapped (Section III-A). TC is used to examine the standard deviation of the random errors, and the correlation coefficient of each product with respect to the unknown true soil moisture.

A. Temporally Averaged Results

Global spatial patterns of m_v products were obtained by temporally averaging the almost 3-years-period gridded m_v

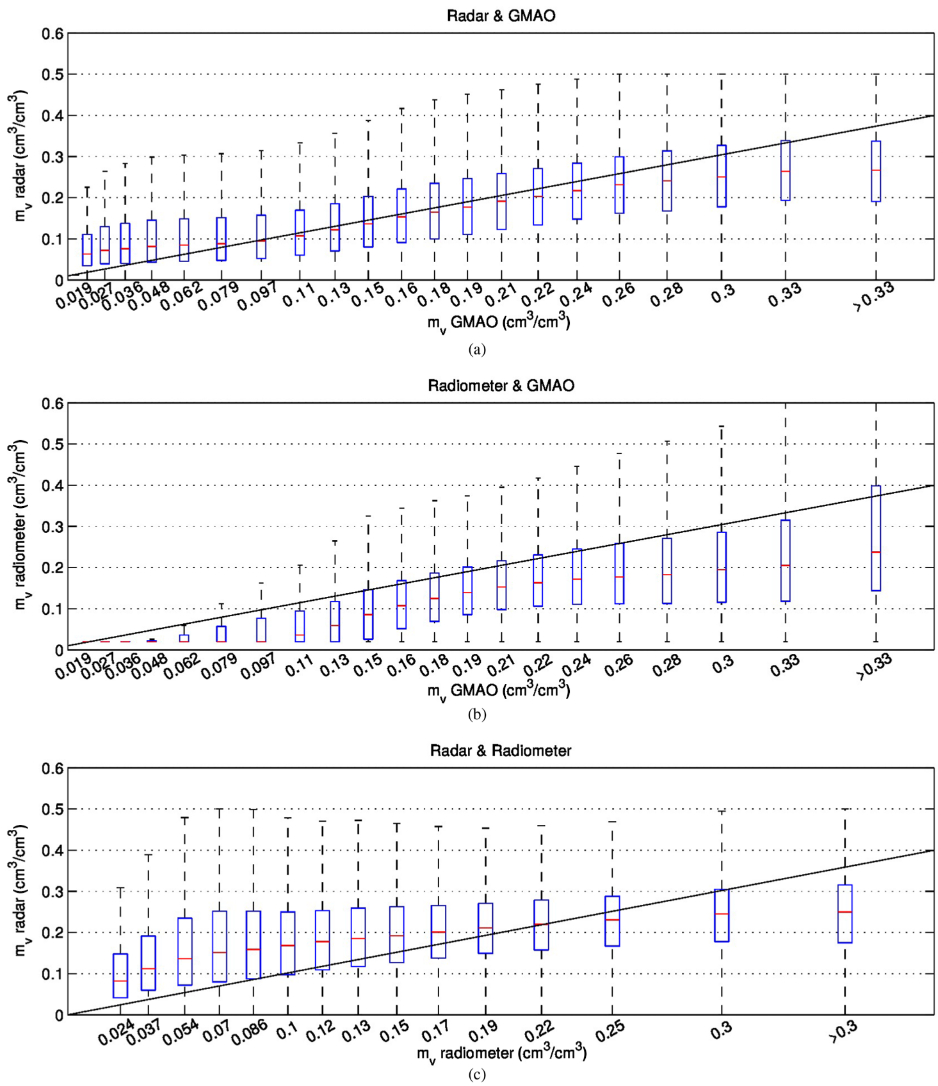

Fig. 4. Boxplots of (a) radar versus GMAO, (b) radiometer versus GMAO, and (c) radar versus radiometer. Solid line is the 1:1 line.

observations (grid defined in Section II-B). Soil moisture m_v products analyzed include: GMAO, the Aquarius radar and radiometer, and National Centers for Environmental Prediction (NCEP). NCEP on the global forecast system (GFS) from the global data assimilation system (GDAS) operational data product at one-degree resolution is provided together with Aquarius L2 soil moisture product collocated to the Aquarius footprints. NCEP is an alternative to GMAO and it is introduced here to consider the errors in the reanalysis data sources. The data are filtered to remove suspected frozen ground conditions during the local cold season.

Global maps of mean m_v are shown in Fig. 5. NCEP exhibits an overall low variability of ($m_v \sim 0.2$ to $0.35\ \text{cm}^3/\text{cm}^3$), with a general wet bias. The wettest area according to NCEP m_v product is Amazon ($m_v \sim 0.4\ \text{cm}^3/\text{cm}^3$), whereas Sahara and Middle East are among the driest regions ($m_v \sim 0.1\ \text{cm}^3/\text{cm}^3$).

For the radar algorithm, the driest regions include southern Africa (Kalahari desert), central and western Australia (Australian desert), central east region in South America, Sahara (specially the southern area), central United States, Patagonian desert, the Arabian peninsula, and Asian deserts (Turkestan, Thar, and Gobi deserts). Areas such as the Amazon and Congo are among the most moist regions in the world; however, the soil wetness condition is clearly underestimated over these regions. This high bias is most likely related to low sensitivity to m_v due to signal attenuation by vegetation cover, thus we expect the radar m_v to have lower retrieval accuracy over densely vegetated regions. Among the wettest regions are rainforest areas in the western coast in Canada and south Alaska, southern Asia rainforest, Japan, northern islands in Canada, Norway, and Siberia.

Compared to GMAO, radar m_v has similar patterns and absolute values over most of: North America, Europe, Asia, and Australia. Nevertheless, a dry bias is observed at northwest Asia, as well as a wet bias at south Asia. The highest discrepancies between both m_v products are observed at high vegetation density areas such as Amazon, Congo, Indonesia, and at freezing soil regions in northern Russia, where a negative bias in RVI was reported in [15].

When considering the radiometer and radar m_v spatial patterns, significant discrepancies are evident in regions such as Amazon, Congo, Alaska, north and southwest areas in Asia,

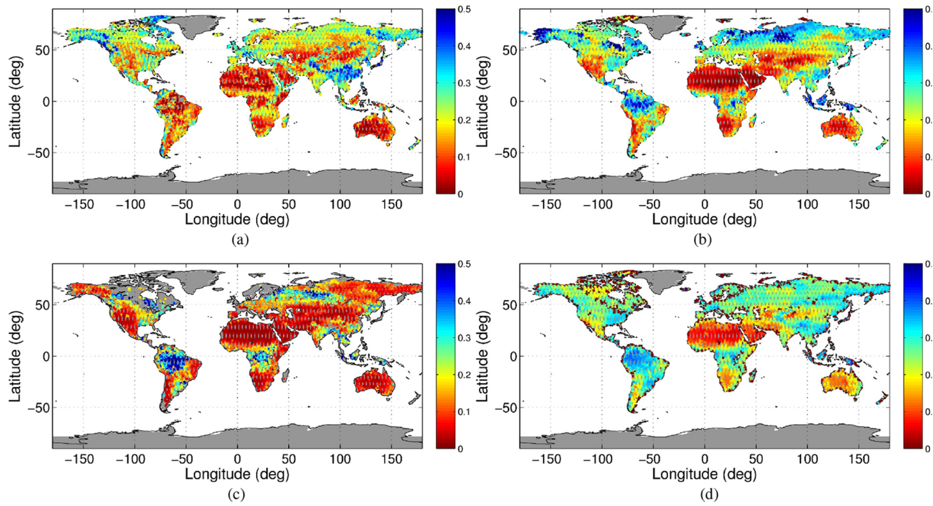

Fig. 5. Spatial patterns (time-averaged) of radar, GMAO, radiometer, and NCEP m_v (cm^3/cm^3) fields.

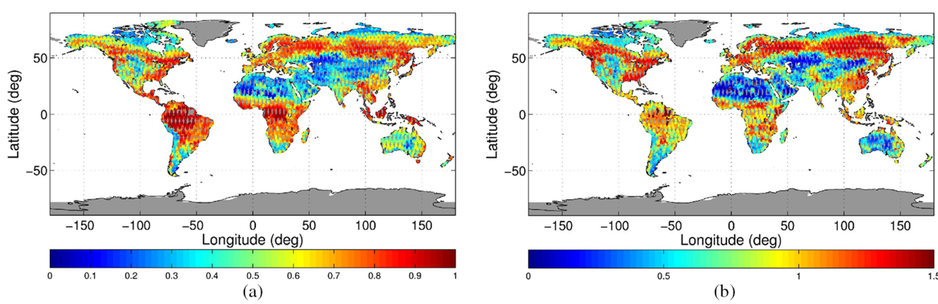

Fig. 6. Spatial patterns (time-averaged) of (a) RVI and (b) retrieved ks.

Europe, and islands in Oceania. On the whole, the global radiometer m_v map shows an apparently excessive dry pattern, except in Amazon, Congo, and northwest Russia, where maximum m_v values are found.

Fig. 6 shows a global map of temporally averaged RVI generated with backscatter observations from the Aquarius. As previously mentioned, areas of dense vegetation (Amazon, Congo, and Indonesia) where RVI was found to have the highest values were regions where radar presents a dryer m_v pattern than GMAO. The opposite was also observed: m_v derived from radar observations exhibit higher values than GMAO m_v product in areas where mean temporal RVI was lower than 0.4. It is important to point out that in areas where RVI values are inaccurate, these inaccuracies will translate to errors on the m_v retrieved by the algorithm developed here. This is the case for central Sahara where RVI is nonzero due to surface roughness, resulting in an overestimation of m_v values (see Fig. 5).

A global map of temporal mean ks can also be retrieved from the radar-only algorithm as shown in Fig. 6. The spatial patterns appear coherent with what might be expected. Low ks values over smooth bare soil such as desert regions (Sahara, Middle East, western Australia, and Chile) and higher ks values over forest regions (boreal forest at Alaska, Canada, and Russia; and tropical rain forest at Amazon, Congo, and New Guinea). From the ks pattern, it seems that areas with high ks correlate with areas that have the highest GMAO and radar m_v discrepancies. This is not surprising since ks and m_v retrievals are not independent in the radar-only algorithm.

The ks values shown in Fig. 6 are considerably higher than those measured in the field at the point-scale (as root-mean square of microtopography). At L-band, ks is expected to be about 0.25 for agricultural soil and up to three to four times this value for extremely rough soils [29]. In particular, the retrieved ks dynamic range is associated with the C parameter in (5). The C value was derived for bare soil based on the results of numerical solutions of Maxwell's equations [16] and is considered fixed to 13.6. Therefore, ks should be considered as an "effective roughness," since in the derivation of C, no subsurface effects were considered. For instance, it was observed by Jackson *et al.* [30] that subsurface rock fragments can cause overestimation on ks values because of the multiple bounce effect. Moreover, in vegetated areas, the distribution of dielectric elements in the canopy manifests themselves as "roughness" in the signal. Thus the roughness shown in Fig. 6 should be regarded as an effective roughness.

B. Extended Triple Collocation

To further evaluate the performance of the radar-only m_v retrieval algorithm, ETC [28] is implemented using m_v anomalies. ETC is an extension of the TC technique used for estimating unknown RMSE of three mutually independent error-prone datasets in the absence of the "true" (noise-free) data source [27]. ETC introduces an equation to TC in order to additionally estimate the correlation coefficient of the measurement system with respect to the unknown target dataset.

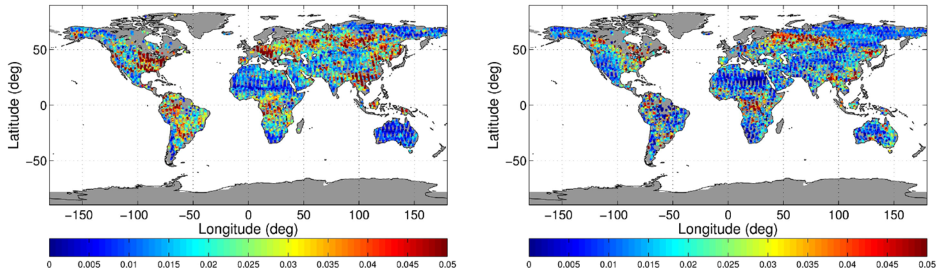

(a) (b)

Fig. 7. Spatial patterns of (a) radar and (b) radiometer ETC RMSE ($\mathrm{cm}^3/\mathrm{cm}^3$) of m_v anomalies.

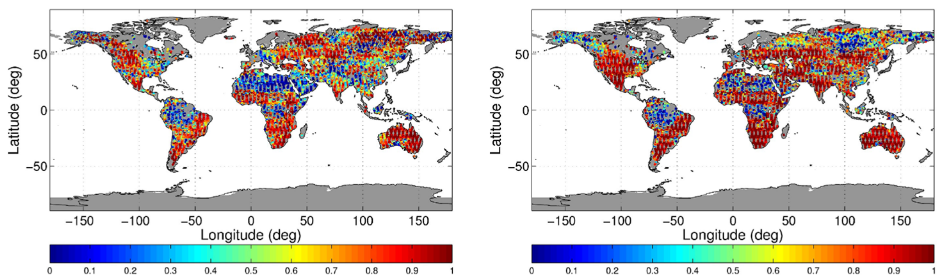

(a) (b)

Fig. 8. Spatial patterns of (a) radar and (b) radiometer ETC correlation of m_v anomalies.

In this study, ETC is implemented using the Aquarius radar, radiometer, and GMAO m_v anomalies. Anomalies were computed by removing the multiyear seasonal climatology from the m_v time series. The climatology was computed as the moving average of the multiyear 31-day period surrounding each day of the year for the whole period of study [31]. Since ETC was computed with m_v anomalies, performance metrics derived from this analysis do not consider errors in the mean seasonal cycle.

Fig. 7 shows global maps of RMSE estimate for radar and radiometer m_v anomalies derived from ETC. Overall, very low RMSE (<0.05 $\mathrm{cm}^3/\mathrm{cm}^3$) is found in both radiometer- and radar-based retrieval datasets. As expected, regions of highest RMSE values for radar m_v correspond to areas with high RVI (see Fig. 6), whereas areas with little to no vegetation show considerably lower RMSE. In addition, regions such as central United States, Brazil, Sahara, eastern Europe, and southeastern coastal area of Asia are among the areas where radar retrievals have a higher RMSE than radiometer. Canada, Argentina, the southern Sahara, Australia, India, and northern Asia exhibit the opposite behavior. It is important to highlight that these results are quite promising since the radar's performance is overall similar to that of the radiometer, despite the fact that radiometer observations are expected to be less noisy than those of the radar, and therefore to retrieve more accurate m_v estimations. Moreover, the radiometer retrieval algorithm uses ancillary parameters that constrain and improve m_v estimation, whereas the radar-only algorithm described in this study uses no extra information, but only backscatter measurements.

Correlation coefficients calculated through ETC are shown in Fig. 8. Radar m_v shows higher correlation over areas including north Asia, Canada, Alaska, most of Australia, and Central Africa. On the other hand, regions with lowest correlation are characterized by having extreme RVI values (bare soil: Sahara and Middle East deserts, and maximum vegetation: Amazon). In the case of the radiometer-based retrievals, correlation coefficients are higher than those of radar-based retrievals over south Asia, southeast North and South America and south Africa. Similar to the radar, radiometer correlations are lowest in areas such as the Amazon, Sahara, and permafrost areas (Alaska and northeast Russia).

Estimation of the precision of ETC performance metrics is calculated through bootstrapping, a statistical significance test that computes the sampling distribution of an estimator by sampling with replacement from the original sample. In this analysis, 1000 bootstrap replicates were drawn to compute ETC metrics. The standard deviation of the ETC estimates derived from the 1000 bootstrap samples was found to be lower than 0.01 $\mathrm{cm}^3/\mathrm{cm}^3$ for RMSE and 0.25 for correlation coefficient in areas such as the Amazon, central Africa, and northeast Asia, whereas the lowest standard deviation were observed in Australia, Sahara, North America, and southern South America. Given these estimation errors, the ETC metric values can be considered highly reliable.

Global ETC performance metrics are stratified by dominant RVI and shown in Fig. 9. Both the radar-based and radiometer-based retrievals have comparable RMSE and correlation at different levels of vegetation cover.

The correlation coefficient of radiometer m_v anomalies remains close to 0.8 and drops significantly for densely vegetated areas reaching 0.4. The correlation coefficient of radar anomalies varies more with RVI. The differences between the radar and radiometer correlation coefficients observed for low RVI values but not for the equivalent RMSEs highlight the importance of validating with multiple metrics. Since the radar and radiometer RMSEs are similar for low RVI values, the differences in correlation coefficients are likely due to differences in sensitivity to soil moisture between the radar and radiometer

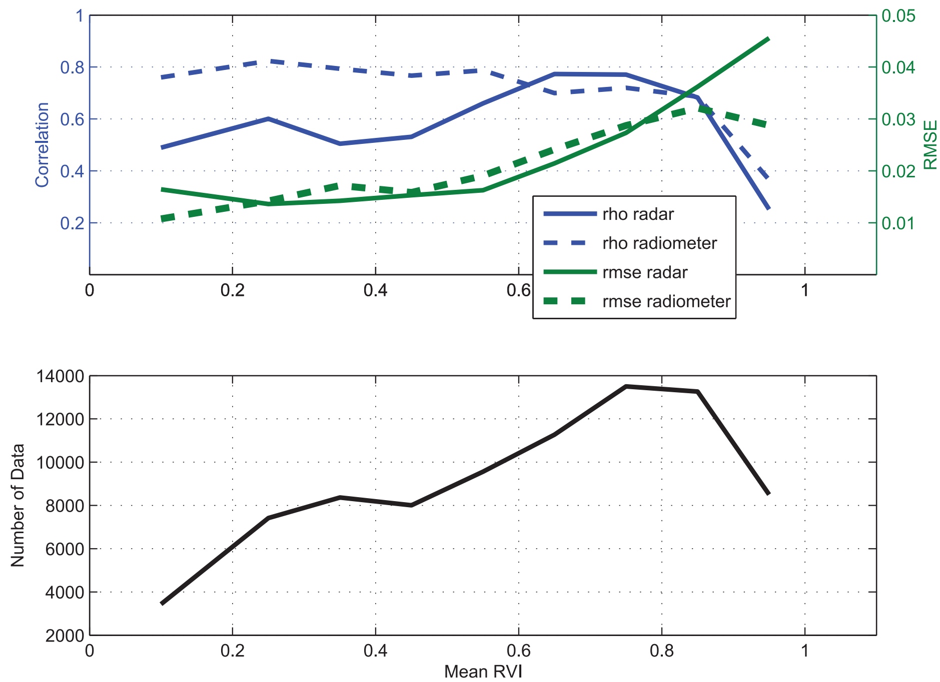

Fig. 9. Statistics [correlation and RMSE (cm^3/cm^3)] derived from ETC stratified by vegetation level (RVI) (upper panel) and number of pixels in each stratification (lower panel).

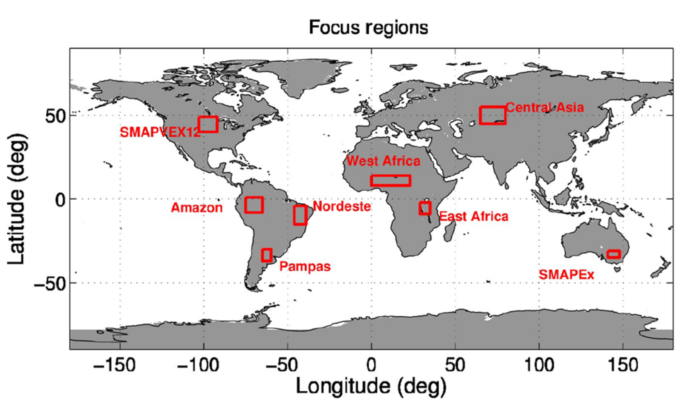

Fig. 10. Focus regions location map.

under low vegetation conditions (see (10) of [27]). The qualitative similarity between the RVI-sample size curve [Fig. 9(b)] and the RVI-rho radar curve [Fig. 9(a)] suggests part of the difference between radar and radiometer correlation coefficients at low RVI values may, therefore, be due to underestimation of the radar product's $Sensitivity$ parameter. It can be seen from the figure that radar and radiometer RMSE exhibit similar behavior. RMSE increases with increasing RVI, from 0.015 cm^3/cm^3 to 0.03 and 0.04 cm^3/cm^3, for radar and radiometer, respectively.

C. Focus Regions Time Series

In addition to the global spatial analysis of m_v products, a diverse number of target regions around the world are selected for closer evaluation of the temporal behavior of m_v at the sites. The locations of the eight selected sites are shown in Fig. 10.

Target sites include both sparse and dense vegetation areas, and soils in dry and wet conditions. In each focus region, radar, radiometer, and GMAO m_v were weekly averaged. Results are shown in Fig. 11 (lower panels). Average MERRA daily rainfall is also included as vertical bars (black) on the time-axis.

Overall, the three m_v products capture well the precipitation peaks in all focus regions. Furthermore, time series in most of the regions correlate strongly with each other. However, some discrepancies are observed. For instance, although the radar m_v's dynamic range in the Amazon follows the seasonality of rain events, it exhibits a dry bias with respect to the remaining two datasets. Note that over densely vegetated regions, it is expected for radar retrieval to have poor performance, since the backscatter signal may not penetrate the dense canopy to the ground at L-band and volume scattering is dominant (further discussion below, after the introduction of the upper panels in Fig. 11).

The upper panels in Fig. 11 partition the total VV polarization signal measured by the Aquarius scatterometer into the constitutive components as predicted by the retrieval algorithm. The black line is weekly mean σ_{VV} (dB) observations from the Aquarius, brown, and green shading represent roughness and vegetation effect on contributions to σ_{VV}, and red to blue colors indicate soil moisture contribution to σ_{VV}, from 0.02 to 0.5 cm^3/cm^3, respectively. Contributions were isolated by using (5) and assumptions on RVI and m_v. The roughness effect is computed when $m_v = 0.02$ cm^3/cm^3 and RVI $= 0$. Hence, the roughness contribution is

$$\sigma_{VV}^{ks} = [1+\log(1+ks)]S_s * 0.02^{0.3} + \sigma_{VV}^{s} + C\log(1+ks). \quad (6)$$

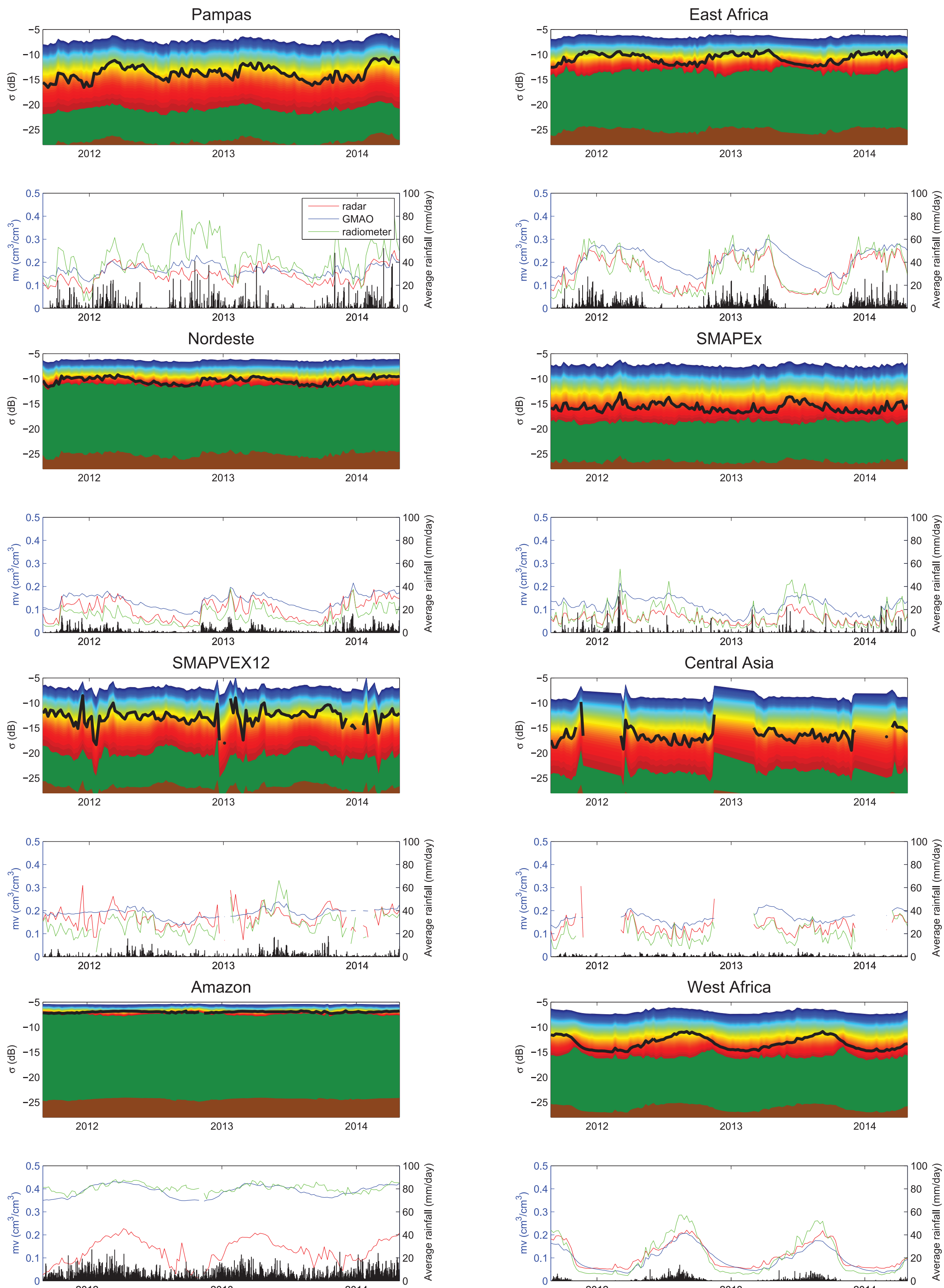

Fig. 11. Focus regions time-series of σ_{VV} (upper panels) and m_v (lower panels). Upper panels: color shading represents roughness (brown), vegetation (green) and soil moisture (blue to red) contributions to σ_{VV}. The black line is σ_{VV} observations from the Aquarius. Lower panels: radar (red), radiometer (green) and GMAO (blue) m_v time series, and average daily rainfall (black bars) obtained from GMAO.

The vegetation effect added to the roughness contribution was obtained by considering $m_v = 0.02\ \mathrm{cm}^3/\mathrm{cm}^3$, thus

$$\sigma_{VV}^{RVI+ks} = \{RVI\gamma + (1 - RVI)[1+\log(1+ks)]S_s\} * 0.02^{\lambda} + RVI\sigma_{VV}^{vf} + (1-RVI)[\sigma_{VV}^{s} + C\log(1+ks)]. \quad (7)$$

Finally, the soil moisture contribution is accounted for by ranging m_v values from 0.02 to 0.5 $\mathrm{cm}^3/\mathrm{cm}^3$ in (5). The ability to isolate the time-varying contributions of volume scattering and effective surface roughness to the total backscatter signal shown in Fig. 11 can also be used to define the normalizing ranges of index algorithms used to estimate relative soil saturation [32]. Exploiting the multiangular characteristic of ERS system, Wagner *et al.* [32] perform a sensitivity analysis of σ to vegetation at different incidence angles. They developed an m_v retrieval algorithm for ERS based on a relative moisture content index, and it was adopted afterward in the ASCAT operational m_v retrieval. Similar to the m_v retrieval algorithm developed here, it relies on the existence of limiting cases (bare and vegetated soils in dry and wet conditions) during a calibration period, and the m_v retrieved is relative to these extreme cases. However, there are several assumptions in [32] that are significantly different from the hypotheses of the methodology developed here, including: 1) a linear relation is considered between $\sigma(40°)$ (dB) and m_v; 2) soil roughness and land cover are temporally invariant; and 3) vegetation phenology influences σ identically from year to year, and is represented by a single harmonic of annual cycle.

Returning to the Amazon focus-region, it is evident that volume scattering by the dense vegetation is by far the dominant signal and dominant contributor to the backscatter cross-section. The effect of surface reflectivity and soil moisture is close to the noise level of the instrument. As a result, the retrieval algorithm performance under dense vegetation cover is suspect.

The sharp discontinuities in the Central Asia and SMAPVEX12 time-series correspond to freeze/thaw events. The pixels with suspected frozen conditions must be filtered or else they become a major source of error and inconsistency.

A different situation was found in the Pampas region, where radiometer m_v displayed the highest dynamic range, whereas GMAO and radar time series are more similarly related.

In areas such as east Africa, Nordeste, SMAPEx, and central Asia, GMAO m_v behaves as an upper limit envelope with the lowest variability, while the remaining m_v time series are in good agreement with each other.

Note that of all the sites, SMAPVEX12 was the one that displayed the highest degree of discrepancy between the three products: whereas GMAO m_v exhibits low to almost no dynamic range, radiometer m_v has the highest sensitivity to rain peaks and radar m_v appears to have an overestimated sensitivity to low rain events at the beginning of the period under study. The SMAPVEX12 focus region is an agricultural area with strict management of the vegetation with planting and harvest events. The GMAO land surface model does not take into account such rapidly changing vegetation conditions. Fig. 11 shows that during the crop growth season (mid-summer) both the radar- and radiometer-based retrievals follow each other closely and show a marked drydown as growing crops take up soil moisture. The GMAO estimates of the SMAPVEX12 soil moisture time-series, however, exhibit a much slower drydown during the summer months most likely because the rapidly changing vegetation is not included in the landsurface modeling.

In the West Africa time series, it is evident that rain events precede vegetation growth. Backscatter is affected by both the growing vegetation and the soil moisture. Therefore, during the decaying phase of σ_{VV} when vegetation contribution starts to increase, soil moisture contribution is distorted approximately following vegetation contribution. This behavior tends to alter the vegetation effect on the signal, making the retrieved m_v decrease more rapidly than σ_{VV}. Over the West Africa region, the radar m_v signal time-series matches the one of the radiometer m_v.

Furthermore, as expected, vegetation contribution to σ_{VV} is of most importance in the Amazon, Nordeste, and East Africa, in that order.

In addition, the vegetation contribution captures crop seasonality in agricultural areas such as Pampas and SMAPVEX12 (phase-shifted because of the North/South hemisphere difference).

D. Robustness of the Iteration Procedure to Initial Guess Values

All results shown so far were obtained for m_v retrieved using the converged end-member parameters considering as initial guess values the end-members derived from SMAPVEX08 datasets [1]. However, in Section II-C, it was shown that differences among the initial guess parameters of the iteration procedure leads to different converged end-member values. Although in Fig. 3 the convergence of the *Sensitivity* end-members (γ and S_s) may not seem robust, converged *Intercept* end-member values are fairly stable. This feature is important because ks is estimated using σ_{HH}^{s} and σ_{VV}^{s}. Thus, ks estimation proves to be robust to changes in initial guess values.

Given that the relative dynamic of observed σ_{VV} is related to ks and m_v, and not to *global* end-member parameters, having different S_s and γ values will mostly impact m_v as a scale factor. To examine the bias between retrieved m_v using different initial parameters, the standard deviation across the ensemble of temporal mean m_v is shown in Fig. 12. In particular, differences are larger at areas with higher RVI, where differences in γ have higher impact on retrieved m_v, and where m_v retrieval is expected to have larger RMSE. Thus, the impact of γ on the m_v retrieval is larger than S_s, even if S_s convergence may seem less robust (see Fig. 3).

To further examine the robustness of m_v dynamics to converged end-members, we analyzed the standard deviation across the ensemble of the m_v anomalies. Standard deviation across the ensemble of m_v anomalies captures the uncertainty introduced into the m_v retrievals by uncertainties in the exact values of the end-member converged parameter sets. The inset figure in Fig. 13 shows a histogram of the ensemble standard deviation across all pixels and all times. The differences

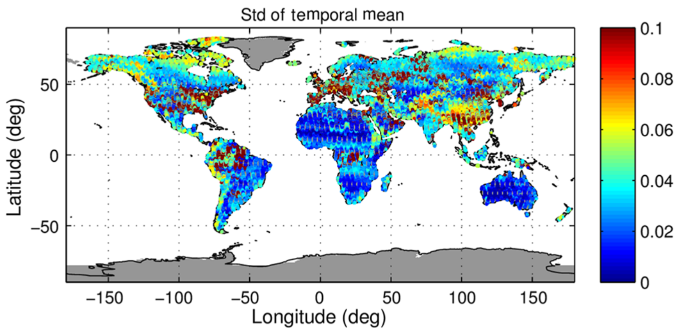

Fig. 12. Standard deviation across ensemble of temporal mean m_v. Ensemble of retrieved m_v is obtained by using different converged end-member values when initializing the iteration procedure with different random guess values.

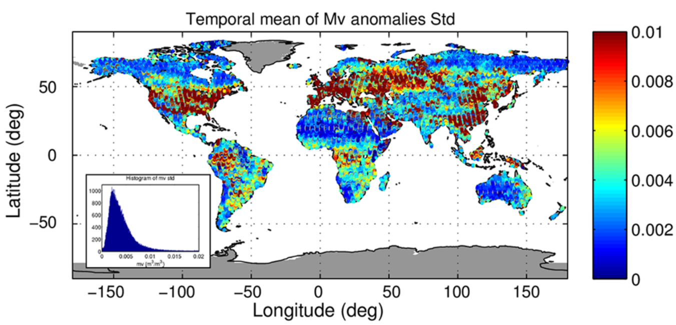

Fig. 13. Histogram of the standard deviation across ensemble of m_v anomalies (inset figure) and map of its temporal mean at each pixel. Ensemble of retrieved m_v is obtained by using different converged end-member values when initializing the iteration procedure with different random guess values.

between m_v anomalies obtained with the set of end-members are significantly small, much smaller than the ETC RMSE values shown in Section III-B. These results imply that the retrieved m_v anomalies are robust to initialization of the iteration procedure. Moreover, a map of the temporally averaged standard deviation across the m_v ensemble at each pixel is shown in Fig. 13. Areas characterized by larger impact of initial end-members on m_v anomalies are also areas with high ETC RMSE. However, the magnitude of ETC RMSE is significantly higher than the ensemble standard deviation. Therefore, uncertainty of the end-member converged parameter values is a minor contributor to the total ETC RMSE.

IV. Conclusion

An implementation of the L-band radar-only soil moisture retrieval algorithm developed by Narvekar *et al.* [1] with 3 years of global scatterometer measurements from the Aquarius is presented and evaluated using two independent datasets. The algorithm has a simple architecture and derivation. It is based on the definition of three limiting cases, i.e., end-members: 1) smooth bare soil; 2) rough bare soil; and 3) maximum vegetation. Parameters for these end-members are global and specific to the L-band radar (owing to resolution, view-angle, etc.). Two radar-derived indices, namely the RVI and the RRI, are used to modulate the parameters for each location at each overpass time among the global end-members. Since the RRI, the RVI and the retrieval algorithm require only radar data, the algorithm is free of the need for ancillary information. Ancillary information, such as land classification and the vegetation and roughness parameters derived from it, is highly uncertain and a major source of error. The classifications are mostly based on optical measurements and not indicative of microwave effects of surface conditions. The proposed algorithm is simple to apply, it can be analytically inverted and most importantly, it does not require any ancillary source of information.

In this paper, an estimation procedure for the end-member parameters is developed in order to apply the algorithm to global space-borne backscatter observations. It performs an iterative search for the optimum parameters that minimize the difference between the observed and estimated σ_{VV} values. Graphically, the methodology attempts to find the three end-points that would best fit all data points in a shape defined by three vertices in the *Sensitivity* and *Intercept* versus RVI plots (see Fig. 1).

Evaluation of the algorithm is carried out using 3 years of global L-band scatterometer observations from the Aquarius/SAC-D. The iterative procedure converges to stable global parameters values (five in number) to retrieve m_v. Several approaches to the evaluation of the m_v retrievals are followed: 1) mean temporal m_v maps are computed for spatial pattern evaluations and comparison with available m_v products (NCEP, GMAO, and the Aquarius radiometer); 2) ETC is implemented to derive performance metrics (RMSE and correlation coefficient); and 3) m_v time series are analyzed over selected focus regions.

Overall, the radar- and radiometer-based m_v RMSE are comparable (<0.05 $\mathrm{cm}^3/\mathrm{cm}^3$). There is a tendency for radar-based retrieval RMSE to increase with RVI. Correlation coefficients are higher for radar-based retrievals at moderate vegetation areas. The radar m_v correlation values are lower than those for the radiometer, over light to moderate vegetated areas. Possible sources of the performance shortfall include the following, which could be the focus of follow-on studies. The two bare soil end-members are not so clearly defined as the maximum vegetation end-member. There are not many points with RVI close to 0 at the Aquarius footprint scale and at different roughness conditions. Moreover, data points at this edge of the shape are rather sparse. Second, low vegetation regions (where σ_{HV} is very low) are prone to have strong positive biases in RVI due to its high sensitivity to additive cross-polarized calibration bias [15].

When RVI increases, σ_{VV} sensitivity to m_v decreases. Therefore, densely vegetated areas are expected to have larger errors of m_v retrieval. This is the case for the Amazon rainforest where a strong dry bias is observed, probably related to low accuracy in the estimated *Intercept*. Given the observed compensation between the parameter values during the iterative calibration process, errors of the estimated *Sensitivity* might lead to errors in the *Intercept*.

As a final comment, the radar-only retrieval algorithm accuracy is comparable to the radiometer-based one. This is quite promising because the advantage of radar in the context of forthcoming missions (SMAP and SAOCOM) is higher spatial resolution. Furthermore, the algorithm does not require ancillary information, which may be unavailable or error-prone. In contrast, the radiometer retrieval uses ancillary information, in particular, MODIS normalized difference vegetation index, a land cover map and NCEP GFS soil surface temperature.

REFERENCES

[1] P. Narvekar, D. Entekhabi, S. Kim, and E. Njoku, "Soil moisture retrieval using L-band radar observations," *IEEE Trans. Geosci. Remote Sens.*, vol. 53, no. 6, pp. 3492–3506, Jun. 2015.

[2] K. C. Kornelsen and P. Coulibaly, "Advances in soil moisture retrieval from synthetic aperture radar and hydrological applications," *J. Hydrol.*, vol. 476, pp. 460–489, 2013.

[3] S.-B. Kim, L. Tsang, J. T. Johnson, S. Huang, J. J. van Zyl, and E. G. Njoku, "Soil moisture retrieval using time-series radar observations over bare surfaces," *IEEE Trans. Geosci. Remote Sens.*, vol. 50, no. 5, pp. 1853–1863, May 2012.

[4] L. Zhou, L. Tsang, V. Jandhyala, Q. Li, and C. H. Chan, "Emissivity simulations in passive microwave remote sensing with 3-D numerical solutions of maxwell equations," *IEEE Trans. Geosci. Remote Sens.*, vol. 42, no. 8, pp. 1739–1748, Aug. 2004.

[5] R. Rahmoune, P. Ferrazzoli, Y. H. Kerr, and P. Richaume, "SMOS level 2 retrieval algorithm over forests: Description and generation of global maps," *IEEE J. Sel. Topics Appl. Earth Observ. Remote Sens.*, vol. 6, no. 3, pp. 1430–1439, Jun. 2013.

[6] J. Wickel, T. J. Jackson, and A. E. F. Woo, "Multitemporal monitoring of soil moisture with RADARSAT SAR during the 1997 Southern Great Plains hydrology experiment," *Int. J. Remote Sens.*, vol. 22, no. 8, pp. 1571–1583, May 2001.

[7] N. Holah, N. Baghdadi, M. Zribi, A. Bruand, and C. King, "Potential of ASAR/ENVISAT for the characterization of soil surface parameters over bare agricultural fields," *Remote Sens. Environ.*, vol. 96, no. 1, pp. 78–86, 2005.

[8] Y. Oh, K. Sarabandi, and F. T. Ulaby, "An empirical model and an inversion technique for radar scattering from bare soil surfaces," *IEEE Trans. Geosci. Remote Sens.*, vol. 30, no. 2, pp. 370–381, Mar 1992.

[9] P. C. Dubois, J. Van Zyl, and T. Engman, "Measuring soil moisture with imaging radars," *IEEE Trans. Geosci. Remote Sens.*, vol. 33, no. 4, pp. 915–926, Jul. 1995.

[10] J. Shi, J. Wang, A. Y. Hsu, P. E. O'Neill, and E. T. Engman, "Estimation of bare surface soil moisture and surface roughness parameter using L-band SAR image data," *IEEE Trans. Geosci. Remote Sens.*, vol. 35, no. 5, pp. 1254–1266, Sep. 1997.

[11] E. Santi, S. Paloscia, S. Pettinato, and G. Fontanelli, "A prototype ann based algorithm for the soil moisture retrieval from L- band in view of the incoming SMAP mission," in *Proc. 13th Spec. Meeting Microw. Radiom. Remote Sens. Environ. (MicroRad)*, Mar. 2014, pp. 5–9.

[12] Y. Kim and J. J. van Zyl, "A time-series approach to estimate soil moisture using polarimetric radar data," *IEEE Trans. Geosci. Remote Sens.*, vol. 47, no. 8, pp. 2519–2527, Aug. 2009.

[13] M. Arii, J. J. van Zyl, and Y. Kim, "A general characterization for polarimetric scattering from vegetation canopies," *IEEE Trans. Geosci. Remote Sens.*, vol. 48, no. 9, pp. 3349–3357, Sep. 2010.

[14] S. Yueh, S. Dinardo, S. Chan, E. Njoku, T. Jackson, and R. Bindlish, "Passive and active L-band system and observations during the 2007CLASIC campaign," in *Proc. IEEE Int. Geosci. Remote Sens. Symp. (IGARSS)*, Jul. 2008, vol. 2, pp. II-241–II-244.

[15] K. A. McColl, D. Entekhabi, and M. Piles, "Uncertainty analysis of soil moisture and vegetation indices using aquarius scatterometer observations," *IEEE Trans. Geoscience Remote Sens.*, vol. 52, no. 7, pp. 4259–4272, Jul. 2014.

[16] S. Huang, L. Tsang, E. G. Njoku, and K. S. Chan, "Backscattering coefficients, coherent reflectivities, and emissivities of randomly rough soil surfaces at L-band for SMAP applications based on numerical solutions of maxwell equations in three-dimensional simulations," *IEEE Trans. Geosci. Remote Sens.*, vol. 48, no. 6, pp. 2557–2568, Jun. 2010.

[17] F. T. Ulaby, R. K. Moore, and A. K. Fung, *Microwave Remote Sensing: Active and Passive*. Reading, MA, USA: Addison-Wesley, 1986, vol 3.

[18] Y. Du, F. T. Ulaby, and M. C. Dobson, "Sensitivity to soil moisture by active and passive microwave sensors," *IEEE Trans. Geosci. Remote Sens.*, vol. 38, no. 1, pp. 105–114, Jan. 2000.

[19] Y. Oh, "Quantitative retrieval of soil moisture content and surface roughness from multipolarized radar observations of bare soil surfaces," *IEEE Trans. Geosci. Remote Sens.*, vol. 42, no. 3, pp. 596–601, Mar. 2004.

[20] J. R. Wang, E. T. Engman, T. Mo, T. J. Schmugge, and J. C. Shiue, "The effects of soil moisture, surface roughness, and vegetation on L-band emission and backscatter," *IEEE Trans. Geosci. Remote Sens.*, vol. GE-25, no. 6, pp. 825–833, Nov. 1987.

[21] F. T. Ulaby and P. P. Batlivala, "Optimum radar parameters for mapping soil moisture," *IEEE Trans. Geosci. Electron.*, vol. 14, no. 2, pp. 81–93, Apr. 1976.

[22] R. Bindlish and T. Jackson, "Aquarius l2 swath single orbit soil moisture. version 2," NASA DAAC at the National Snow and Ice Data Center, Boulder, CO, USA, 2013.

[23] R. Reichle, "The SMAP nature v03 data product," personal communication, 2014.

[24] R H Reichle *et al.*, "Assessment and enhancement of MERRA land surface hydrology estimates," *J. Clim.*, vol. 24, no. 24, pp. 6322–6338, 2011.

[25] R. H. Reichle *et al.*, "Observation-corrected precipitation estimates in GEOS-5," Goddard Space Flight Center, NASA, Greenbelt, MD, USA, Tech. Rep. TM-2014-104606, 2014, vol. 35.

[26] G. J. M. De Lannoy, R. D. Koster, R. H. Reichle, S. P. P. Mahanama, and Q. Liu, "An updated treatment of soil texture and associated hydraulic properties in a global land modeling system," *J. Adv. Model. Earth Syst.*, vol. 6, pp. 957–979, 2014.

[27] A. Stoffelen, "Toward the true near-surface wind speed: Error modeling and calibration using triple collocation," *J. Geophys. Res. Oceans*, vol. 103, no. C4, pp. 7755–7766, 1998.

[28] K. A. McColl, J. Vogelzang, A. G. Konings, D. Entekhabi, M. Piles, and A. Stoffelen, "Extended triple collocation: Estimating errors and correlation coefficients with respect to an unknown target," *Geophys. Res. Lett.*, vol. 41, pp. 6229–6236, 2014.

[29] M Davidson, T. L. Toan, F. Mattia, G. Satalino, T. Manninen, and M. Borgeaud, "On the characterization of agricultural soil roughness for radar remote sensing studies," *IEEE Trans. Geosci. Remote Sens.*, vol. 38, no. 2, pp. 630–640, Mar. 2000.

[30] T. J. Jackson, K. G. Kostov, and S. S. Saatchi, "Rock fraction effects on the interpretation of microwave emission from soils," *IEEE Trans. Geosci. Remote Sens.*, vol. 30, no. 3, pp. 610–616, May 1992.

[31] D. G. Miralles, W. T. Crow, and M. H. Cosh, "Estimating spatial sampling errors in coarse-scale soil moisture estimates derived from point-scale observations," *J. Hydrometeorol.*, vol. 11, no. 6, pp. 1423–1429, 2010.

[32] W. Wagner, G. Lemoine, M. Borgeaud, and H. Rott, "A study of vegetation cover effects on ERS scatterometer data," *IEEE Trans. Geosci. Remote Sens.*, vol. 37, no. 2, pp. 938–948, Mar. 1999.

Cintia A. Bruscantini (S'10) received the Bachelor's degree (with Hons.) in electronic engineering from the National University of Mar del Plata, Buenos Aires, Argentina, in 2010. She is currently pursuing the Ph.D. degree in engineering from the University of Buenos Aires, Buenos Aires, Argentina.

She works with the Instituto de Astronomía y Física del Espacio (IAFE), Buenos Aires, Argentina. She is part of the calibration team of the microwave radiometer MWR on board the SAC-D. She is funded by the Consejo Nacional de Investigaciones Científicas y Técnicas (CONICET). Her research interests include OSSEs, remote sensing of soil moisture and instrument prototype developments.

Alexandra G. Konings (S'12) received the S.B. degree in environmental engineering science from Massachusetts Institute of Technology (MIT), Cambridge, MA, USA, the M.S. degree in environmental science from Duke University, Durham, NC, USA, and the Ph.D. degree from MIT, in 2009, 2011, and 2015, respectively.

She is currently a Postdoctoral Fellow with Columbia University and will be an Assistant Professor with the Department of Earth System Science, Stanford University starting in Fall 2016. Her research interests include microwave remote sensing of the land surface, ecohydrology, and land-atmosphere interactions. Dr. Konings was the recipient of the National Science Foundation Graduate Research Fellowship in 2009, and the National Aeronautics and Space Administration Earth and Space Science Fellowship in 2012.

Parag S. Narvekar (M'13) received the Ph.D. degree in polarimetric microwave remote sensing of land and snow/ice from the University of Bremen, Bremen, Germany, in 2007.

Since 2011, he has been with the Massachusetts Institute of Technology, Cambridge, MA, USA. From 2011 to 2014, he was also jointly appointed with the Jet Propulsion Laboratory, CA, USA, as a Research Affiliate. Earlier, he worked with different institutes, including the U.S. Department of Agriculture, MD, USA, the City University of New York, New York, NY, USA, the University of Bremen, Bremen, Germany, and the Indian Institute of Technology Bombay, Mumbai, India. His research interests include the application and development of remote sensing technology for estimating land surface geophysical quantities in real time needed in a variety of agricultural and hydrological applications.

Dr. Narvekar has served on the NASA and National Science Foundation grant review panels. He was the recipient of the Massachusetts Institute of Technology Big Data Educational Fellowship.

Kaighin A. McColl (S'09) received the Bachelor's degree (with Hons.) in environmental engineering and the Bachelor of Science degree in applied mathematics from the University of Melbourne, Parkville, Vic., Australia, in 2009. He is currently pursuing the Ph.D. degree in civil and environmental engineering at Massachusetts Institute of Technology, Cambridge, MA, USA.

He was funded by the National Science Foundations Graduate Research Fellowship Program. His research interests include boundary-layer meteorology, landinteractions, and remote sensing of soil moisture and vegetation.

Dara Entekhabi (M'04–SM'09–F'15) received the Bachelor's and Masters' degrees in geography from Clark University, Worcester, MA, USA, in 1983, 1984, and 1987, respectively, and the Doctoral degree in civil engineering from the Massachusetts Institute of Technology (MIT), Cambridge, MA, USA, in 1990.

He is currently a Professor with the Department of Civil and Environmental Engineering and the Department of Earth, Atmospheric and Planetary Sciences, MIT. He is the Science Team Lead for the National Aeronautics and Space Administrations Soil Moisture Active and Passive (SMAP) mission that was launched January 31, 2015. His research includes terrestrial remote sensing, data assimilation, and coupled landsystems modeling.

Dr. Entekhabi is also a Fellow of the American Meteorological Society and the American Geophysical Union.

Francisco M. Grings received the B.S. degree from the University of General San Martin San Martin (UNSAM), San Martin, Argentina, and the Ph.D. degree in physics from the University of Buenos Aires (UBA), Buenos Aires, Argentina, in 2008.

He is a Research Member of Consejo Nacional de Investigaciones Cientıficas y Tecnicas (CONICET), Santa Fe, Argentina, and working with the Instituto de Astronomıa y Fısica del Espacio (IAFE), Buenos Aires, Argentina. His research interests include Bayesian time series retrieval of remotely sensed data, electromagnetic modeling of vegetation and soil and the development of Observing System Simulation Experiments (OSSEs) for future Argentine mission.

Haydee Karszenbaum received the degree in physics from the University of Tennessee, Knoxville, TX, USA.

She was a Research Fellow with the College of Marine Studies, University of Delaware, Newark, Delaware. Since 1980, she has been a Research Member of Consejo Nacional de Investigaciones Científicas y Técnicas (CONICET), Santa Fe, Argentina, a Remote Sensing Specialist, and the Director of the Remote Sensing Group with the Instituto de Astronomía y Física del Espacio (IAFE), Buenos Aires, Argentina. She is currently the PI of national projects and of Space Agencies AO projects.